Verifying the feasibility of using Hand-Held X-ray fluorescence spectrometer to analyze Linqing brick: evaluation of the influencing factors, assessing reliability, and providing scientific advice

Zexuan Chen (chenzexuan@tju.edu.cn)
Tianjin University https://orcid.org/0000-0003-1043-880X
Long Zhang
Tianjin University
Feng Hou
Tianjin University
Jialiang Xie
Tianjin University

Research article

Keywords: HH-XRF, Linqing brick, reliability, accuracy, ICP-OES

Posted Date: August 19th, 2020

DOI: https://doi.org/10.21203/rs.3.rs-30789/v2

Version of Record: A version of this preprint was published on September 21st, 2020. See the published version at https://doi.org/10.1186/s40494-020-00437-5.

Abstract

Linqing brick is quite popular in Chinese history. Currently, identifying the origin of Linqing brick is an important issue to be studied in the field of archeology and architectural history in China. Hand-Held X-ray fluorescence (HH-XRF) spectrometry enables the in-situ determination of the main elements in Linqing brick in a rapid non-destructive manner. HH-XRF is important in identifying the origin of Linqing brick. However, HH-XRF could be influenced by certain factors and may be capable of measuring only the element contents of the surface for the bricks in situ. The present study aimed to verify the reliability of HH-XRF and to systematically evaluate the different factors influencing measurement precision and accuracy so that scientific advice could be provided regarding the usage of HH-XRF for this application. Four experiments were performed to determine the influencing factors and assess the reliability through cross-validation using inductively coupled plasma optical emission spectrometry (ICP-OES). Finally, the influence of the different studied factors was studied, and the reliability of HH-XRF was ensured. The facts to consider about the measurement time, cross validation, criteria to select points, treat surface and getting final data and how to avoid the effect of rain, while using this method, are provided.

1. Introduction

Linqing brick is quite famous in Chinese history. Several architectural heritages have been built mainly by Linqing brick, such as the Forbidden City, the Temple of Heaven, the Ming Tombs, and the Western Qing Tombs [1, 2]. From the beginning of the Ming Dynasty to the end of the Qing Dynasty, Linqing brick had continued to be supplied for the construction and repair of the royal buildings for more than 500 years in Beijing [2, 3]. Linqing brick is the most intuitive material for studying the history of its burning, management, transportation and the history of the construction and repair of the royal buildings in the Ming and Qing dynasties. In 2008, “The manufacturing process of Linqing brick” was selected as the intangible cultural heritage list in China [2].

Currently, the identification of the origin of Linqing brick is an important concern [4, 5]. Several Linqing bricks have been found with inscriptions that contain information regarding their origin [6, 7]. Accurate measurement of the main elemental contents of the Linqing bricks with inscriptions may be significant for the identification of their origin. It could be used to solve some issues about the source of materials for the royal buildings in the Ming and Qing dynasties, which cannot be resolved just through historical documents. In addition, it could also be used to build an elemental database of Linqing brick to enhance the scientific understanding of the material [3].

There are a large number of Linqing bricks with inscriptions located on the ancient buildings, such as Ming Tombs [8]. It is impossible to transport these bricks to the laboratory. Hand-Held X-ray fluorescence spectrometry (HH-XRF) allows the measurement of the elemental contents of bricks in a rapid and non-destructive manner so that the elemental contents could be determined in situ.

HH-XRF has been used in the field of archaeology for several years. For instance, data from HH-XRF were used to divide the sources of obsidian, which assists in addressing the research issues concerning prehistoric mobility, exchange, and social networking in a specific area [9–11]. Besides evaluating the source of obsidian, several other archaeological items were studied using HH-XRF, such as pottery [12, 13], bronze [14, 15], and tiles [16, 17].

However, the accuracy and reliability of HH-XRF could be influenced by certain factors. How to analyze the influencing factors, accuracy, and reliability is the subject of the present research. Many researchers have done research on verifying the accuracy and reliability of HH-XRF in different fields [18–22]. The factors concerned by the researchers in different fields are different. For example, in soil science, researchers care more about measurement time, moisture content of soil, bulk sample size, and particle size [18]. While in characterizing obsidian sources, researchers were more focused on accuracy and reliability, mainly by comparing HH-XRF values to those from another technique [10, 20]. The effects of different instrument models and different measurement conditions (hand-held versus test stand operation) on the reproducibility of HH-XRF measurements were also considered [22]. Combining the previous research with the characteristics of this application, the main factors considered in this study are measurement time, rain, surface contamination, and homogeneity. Such factors are quite important in this application. Increasing the count time could increase the possibility that a series of measurements on the same specimen will yield similar results [23]. If an inappropriate measurement time is used, the element contents would be quite different, even if the same point is measured several times. The rainy weather is also an issue, which influences the data, especially for in-situ measurement. As in this case, the photoelectric absorption and scattering increase that leads to higher limits of detection and reduced apparent content [18]. Further, for in-situ measurement, only points on the surface can be considered, which might be affected by several factors. Therefore, it is very important to reduce the effect of surface contamination. The volume of the brick is large, and the contents at different points on the surface of the same brick are different [24]. How to choose points? How many points to choose? How to deal with the data of these points to get final data representing the content of the brick? These factors are addressed in the present study. Four experiments were performed to assess these factors, and the reliability of the instrument was assessed through cross-validation using inductively coupled plasma optical emission spectrometry (ICP-OES).

2. Materials And Methods

2.1 Instrument

The instrument used in the present study was Niton XL2–960 GOLDD XRF Analyzer equipped with an Ag anode tube operating at a maximum of 45 kV and 100 mA and a Geometrically Optimized Large Area Drift Detector (GOLDD). The standard analytical range was up to 30 elements from Mg to U. There are several instrumental modes (Soils, Mining: Cu/Zn, Minging:Ta/Hf) for particular analytes. There are two filters for each irradiation session, including the main range and light range. The filters are set to include the following elements: Main: Ba, Sb, Sn, Cd, Pd, Ag, Sb, Sn, Cd, Pd, Ag, Mo, Nb, Zr, Sr, Rb, Bi, As, Se, Pb, W,

Zn, Cu, Re, Ta, Hf, Ni, Co, Fe, Mn, Cr, V, Ti. Light: Ca, K. Al, P, Si, Cl, S, and Mg. The irradiation area is circular, with 8 mm in diameter.

The Soils mode is more suitable to measure the elements lower than 0.5%, while the Mining mode is more suitable to measure the elements whose contents are greater than 0.5% for the Mining mode was corrected using the fundamental parameters (FP), which can eliminate the interference between the various elements to a large extent. In the X-ray fluorescence spectrum, the peaks of Cu/Zn and Ta/Hf overlap, and a hand-held instrument cannot distinguish them. Therefore, different modes (Mining: Cu/Zn, Minging:Ta/Hf) should be selected according to whether the sample contains Ta/Hf. In the present analysis, the contents of the main elements were higher than 1%, and there was no Ta/Hf in the brick. Therefore, Mining: Cu/Zn was selected as the mode. The total contents of elements were calculated through the built-in algorithm under Mining: Cu/Zn Mode in the HH-XRF. Two filters were used. The instrument was set to the irradiation times of 30 s for each of the main and light filters with the measurement units set to weight percent (%).

A representative brick spectrum obtained from HH-XRF was shown in Fig.S1; 'Counts/Sec' represent the emitted spectrum intensity at each photon energy, so they are the basis for quantitative analysis as well as the built-in algorithm.

2.2 Samples and elements studied

Twenty bricks were used as samples (Table S1).

In experiment 1 and experiment 2, only brick 4 was used. In experiment 3 and cross-validation, all bricks were used.

The main elements studied in the present research were Fe, Ca, K, Al, and Si, whose contents were higher than 1%. In Chinese history, brick and tile have always been mentioned at the same time. Similar to bricks, glazed tiles are also made of mainly clay. Except for the firing temperature, other processes of glazed tiles are similar to bricks. In China, many scholars have studied the characteristics of the main element content of glazed tiles in different regions [25–27]. The elements used include the main elements with the highest content for tile, such as Fe, Ca, Mg, Al, and Si. Yang Guimei et al. distinguished the glazed tiles from Mingzhongdu Site in Fengyang, Minggugong Site in Nanjing and Forbidden City in Bejing by PCA analysis of the main elements [25]. Duan Hongying et al. conducted the main component analysis on 398 glazed tiles from 13 provinces and determined the main element characteristics of glazed tiles from different regions (North China: high silicon and low aluminum; the Central of China: low silicon and high aluminum; the Ningxia province: low silicon and low aluminum; the Liaoning province: high magnesium properties) [27]. According to the research related to the glazed tiles, combined with the element contents of the Linqing brick itself, five elements with the highest content (Fe, Ca, K, Al, and Si) were selected as representatives.

However, in order to determine whether HH-XRF could measure more elements in a good precision, in experiment 1, the elements with a content higher than 0.1% were studied (Fe, Ca, K, Al, Si, Ba, Zr, Mn, Mg, Ti, and Cl). The elements studied in experiment 2, experiment 3, and cross-validation (Fe, Ca, K, Al, and Si) were the main elements considered in the present research.

2.3 Experiment 1: Evaluating the effect of measurement time

The measurement time mainly depends on the HH-XRF Analyzer used, the investigated element, and the content of the investigated element [18]. All studied objects were bricks with a similar composition of elements. Thus, in experiment 1, only 1 brick was used.

In order to evaluate the effect of the measurement time on precision, brick 4 was measured five times at a single point for 60, 90, 120, 150, 180, 210, and 240 s. The point was used for measurement after polishing with a sickle. The relative standard deviation (RSD) value for each element at each measurement time was used to determine the effect of the measurement time on the measurement precision. The US EPA criteria were used to evaluate data quality (Table 1) [28].

2.4 Experiment 2: Evaluating the effect of rain on the day of measurement

Humidity can attenuate the signal of HH-XRF, which depends on the humidity level in the air and the composition of the objects being investigated [29]. In the research, rainfall, temperature, and humidity were constant. So, in experiment 2, only 1 brick was use.

In order to evaluate the effect of rain, HH-XRF measurements were taken before and after washing brick 4 in the rain. The point of measurement was polished with a sickle prior to the measurements (prior to the rain and immediately after rain).

The measurements were performed at 1 point under 10 conditions: prior to the rain, and at 0, 1, 2, 3, 5, 7, 9, and 12 h after rain. The measurement conditions were as follows: rainfall 11.2 mm (1 day), the average temperature of 24.3 °C (1 day), and average humidity of 69.2% (1 day).

2.5 Experiment 3: Evaluating the effect of surface contamination and homogeneity

In order to evaluate the effect of surface contamination, determining the homogeneity, prescribing criteria for point selection, treating surface, and getting final data, the following two experiments were performed.

2.5.1 Experiment 3–1: Uniformity of element distribution on the brick surface: Direct measurement vs. measurement after polishing with a sickle

This experiment evaluated the effect of surface conditions on measurement accuracy. Ten points were selected on each brick surface for the measurement. The measurements were performed under two surface conditions: a direct measurement (DM) and a measurement after polishing with a sickle (MPS).

The uniformity of the element distribution on the brick surface was determined through the RSD of 10 points and (The ratio of the maximum value to the minimum value of 10 points) [30, 31].

2.5.2 Experiment 3–2: The difference in contents between the brick surface and the brick interior

This experiment demonstrated the effect of surface conditions on measurement accuracy and verified the reliability of MPS. Three fresh sections were cut for each brick that was subjected to measurements. The mean elemental contents of these three sections were compared with the mean elemental contents of the previous surface points polished with sickles obtained in experiment 3–1. The Max{Cp,Cs}/Min{Cp,Cs} was used to evaluate the difference between the points and sections (The ratio of the larger content of the point (mean of the 10 points) and section (mean of the 3 sections) to the smaller value of them).

2.6 Cross-validation using inductively coupled plasma optical emission spectrometry

2.6.1 ICP-OES

The bricks were cut into small pieces, and each brick sample was subsequently ground into a fine powder with particle diameter less than 150 μm. Next, total microwave digestion was used to digest the sample. The digested sample (500 mg) was placed in a PTFE reactor with 4 mL (70%), 1 mL (20%), and 2 mL HF (40%). When the foam caused by the decomposition of organic matter disappeared, the container was capped and heated using a microwave digestion instrument, namely, Solutions MD (Beijing Ying'an Meicheng Scientific Instrument company). The heating process was in accordance with a three-stage digestion procedure, which included 3 min to reach a temperature of 150 °C, 5 min at 180 °C, and 5 min to reach 200 °C. After the microwave digestion, the sample was heated in the acid-driven processor. Subsequently, the digest was transferred into a 50-mL flask and brought to volume with MilliQ water. Finally, the diluted digest was analyzed using a device: PerkinElmer ICP-OES Optima 8300. The protocol are all from Sinopharm Chemical Reagent Co.,Ltd.

The instrument equips with two charge-coupled device (SCD) detectors covering the spectral range from 163-782 nm and features a 40 MHz, free-running solid-state RF generator. The Plasma and shear gas are argon. The way of plasma viewing is radial. The RF power is 1200W. The plasma, auxiliary and nebulizing gas flow are 12L/min□0.5L/min□0.5L/min, respectively. The pump rate is 50r/min. The integration time for low WL range and high WL range are 15s and 5s, respectively. The number of replicates per sample is three. The flush time is 30s. There are multiple spectral lines for each element to be tested. The present experiment selected the spectral lines based on the principle of non-interference of spectral line, intensity, and high sensitivity. The selected spectral lines are 259.940 nm for Fe, 371.933 nm for Ca, 766.490 nm for K, 308.215 nm for Mg, 251.612 nm for Si. MilliQ water was used for calibration solutions. Calibration solutions were prepared by serial dilution of monoelement stock solutions of 1000 mg L^{-1}. They included Fe, Ca ,K, Al (0.5 to 2.0mg L^{-1}) and Si (1.0 to 10.0 mg L^{-1}). All solutions were prepared in 1% (v/v) HNO3.

2.6.2 Cross-validation

Deming regression was used in the comparison between HH-XRF and ICP-OES values with HH-XRF placed on the x-axis and ICP-OES on the y-axis. The RSD, coefficient of determination (R^2), and inferential statistics were used to assess a data quality level and compare the relationship between HH-XRF and ICP-OES. The US EPA criteria were used to evaluate data quality (Table 1). If the data quality meeted the requirement of the US EPA criteria, the model was used to data correction for HH-XRF. Rotational (slope, m) and translational (intercept, b) bias were corrected for HH-XRF data by solving for 'y' in 'y = mx+b' for each regression model.

2.7 Quality Assurance

The RSD used in experiment 1 and experiment 3-1 was calculated by dividing the standard deviation by the arithmetic mean of the data from the same measurement time or the data from different points on the same bricks. RSD was used to evaluate the precision of measurement time and the uniformity of the brick surface.

The data generated using HH-XRF were assessed using established criteria through cross-validation (Table 1). The RSD, R^2, and inferential statistics were used to assess a data quality level and compare the relationship between HH-XRF and ICP-OES.

For the linearity level, if the Q3 quality level would to be achieved, the R^2 obtained in the linear regression analysis between HH-XRF and the validation method must be greater than 0.85. For Q2 quality level, R^2 must be greater than 0.7 (Table 1).

In regard to precision requirements, if the Q3 quality level would to be achieved, RSD must be lower than 10%. For Q2 quality level, RSD must be lower than 20% (Table 1).

In regard to inferential statistics, if the Q3 quality level would to be achieved, the slope (m) = 1 (at 95% confidence level), and the y-intercept (b) = 0 (at 95% confidence level) (Table 1). For Q2 quality level, there is no requirement for inferential statistics.

Table 1 Criteria for characterizing data quality (US EPA)

Data quality level	Statistical requirement
Definitive Q3	R = 0.85–1. Relative standard deviation (RSD) ≤ 10%. Inferential statistics (test for gradient of line = 1 and y-intercept = 0) must indicate the two datasets are statistically similar (at the 95% confidence level), i.e., relationship y = x accepted.
Quantitative screening Q2	R = 0.70–1. Relative standard deviation (RSD) <20%. Inferential statistics indicate the two datasets are statistically different; i.e., relationship y = mx or y = mx + c accepted.
Qualitative screening Q1	R = less than 0.70. Relative standard deviation (RSD) > 20%. Inferential statistics indicate that two datasets are statistically different.

3. Results And Discussion

3.1 Evaluating the effect of measurement time on measurements

Some previous studies have demonstrated that increasing the measurement time could achieve higher precision with lower RSD values [32, 33]. However, RSD does not decrease linearly with measurement time, and an extended analysis may not result in tangible improvements in measurement precision [18]. A few studies reported using a fixed measurement time, such as 45 s [34] or 60 s [33].

The present study demonstrated that an optimal measurement time is strongly dependent on the element under investigation (Fig. 1). In the case of Fe, Ca, K, Al, and Si, the main research elements of the present study, RSD was less than 5% for each measurement time (Fig. 1a). In the case of Ba, Zr, and Mn, RSD was less than 10% for each measurement time (Fig. 1b). Therefore, it is suggested that 60 s should be selected as the measurement time for Fe, Ca, K, Al, Si, Ba, Zr, and Mn (Table 2). However, for Mg, RSD was 64.93% when 60 s was selected as the measurement time. The RSD value obviously decreased from 64.93% for 60 s to 11.42% for 180 s. This rule was also applicable to Ti (Fig. 1c). Therefore, it is suggested that 180 s should be selected as the measurement time for Mg and Ti (Table 2). In the case of Cl, RSD values fluctuated, covering a wide range; at certain times, the values were larger than 30%, while at other times, the values were smaller than 5%, without exhibiting any relationship with the corresponding measurement time (Fig. 1d). Therefore, it was inferred that using a Niton XL2–960 GOLDD XRF Analyzer to measure Cl in a Linqing brick is inappropriate.

Table 2 Suggestions for element measurement times using a Niton XL2–960 GOLDD XRF Analyzer

Element	Fe	Ca	K	Al	Si	Ba	Zr	Mn	Mg	Ti
Measurement time	60 s	60 s	60 s	60 s	60 s	60 s	60 s	60 s	180 s	180 s

3.2 Evaluating the effect of rain on measurements

The present study demonstrated that all investigated elements, with the only exception of K, are greatly influenced by rain, and that it takes a long time for the contents of these elements to return to the pre-rain values (Fig. 2). In the present study, it took approximately 7 h to return to the content prior to the rain (Rainfall: 11.2 mm; Average temperature: 24.3 °C; Average humidity: 69.2%).

Therefore, it is crucial to perform the measurements on a sunny day. Meanwhile, if conditions permit, it is better to select measuring bricks located at the inside of the rooms.

If the rain arrives when performing measurements, the measurements must be postponed. When the rain is over, preliminary tests should be conducted on the brick affected by the rain, and comparison should be

made with the content value measured prior to the rain to ensure the reliability and accuracy of the obtained data. In the present study, under certain conditions, it takes 7 h for Fe, Ca, Al and Si to return to the content before the rain. In the meantime, after the rain stopped, the content of these four elements changed greatly every hour until the pre-rain content was restored. Considering the complexity of the rain (rainfall, temperature, humidity, acidity and alkalinity of the rain, etc.), it is difficult to give precise suggestions on how long to start the preliminary tests after rain. Since the content largely changed every hour until the pre-rain content was obtained (Fig 2), taking the preliminary tests every hour after the rain until it returns to the previous value is suggested.

3.3 Evaluating the effect of surface conditions of the brick on measurements, providing a surface treatment method, and verifying the reliability of the method

The bricks on the exterior wall of the ancient buildings have been exposed to the external environment for several hundred years, being affected by several factors such as acid rain, humidity, and dry and wet deposition. These sources of deterioration may promote efflorescence formation, loss of material, and crystalline bloom, particularly on the brick surface. These factors may greatly influence the surface of the brick. Therefore, to improve the precision and accuracy of the measurements, an applicable surface treatment method is required to ensure that the measured data could be used to represent the element content of the entire brick.

3.3.1 Evaluating the uniformity of element distributions on brick surfaces: DM vs. MPS

It is clear that, regardless of the element under investigation, using MPS may cause the contents between every point on the same brick to become closer (Table S2-S6). For Fe and Ca, the RSD calculated from 10 points obtained by MPS is lower than the value obtained by DM for every brick in the experiment (Table S2, S3). Except for some special cases (K brick5; Al brick 3; Si brick3 and brick 14), the rule was also suitable for K, Al and Si (Table S4-S6). Although the RSD for MPS is a little larger than DM for these special cases, the differences between them is quite small and the uniformity of 10 points is good for both MPS and DM (Table S4-S6). After using MPS, the uniformity of surface element contents was significantly improved. and the RSD calculated from the 10 points are used to evaluate the uniformity. As observed in previous studies, if the value of is lower than 1.3 and RSD is lower than 10%; the uniformity is acceptable [31]. After using MPS to treat the surface, the RSD calculated from 10 points of all the bricks investigated were lower than 10% for Fe, K, Al, Si (Table S2, Table S4-S6). The rule was also suitable for Ca, except for brick 5, brick 10 and brick 18 (Table S3). For the , only 5 special cases did not show the value lower than 1.3% (Ca: brick 1, brick 5, brick 10 and brick 18; K: brick 18).

For the objects with large volume and inhomogeneity, measuring multiple points and using the average as the final measurement value is recommended as an effective method [24, 30]. In the present study, only a few special cases cannot meet the requirement of the uniformity (RSD%10%, %1.3%). For these special cases, the differences between the different points of the same brick were still large even after using MPS, which might be caused by the content distributions in the bricks itself. Therefore, the values were discarded.

In order to ensure the accuracy of the measurements, 10 points must be selected on each brick for measurement. Each point must be polished with a sickle prior to performing the measurement. After the measurement, the uniformity should meet the requirement, using the mean content of the 10 points to represent the elemental content of the brick. The specific values, whose uniformity did not meet the requirements, were deleted.

3.3.2 Evaluating the content differences between brick surfaces and interiors

Whether the mean value of ten surface points can roughly represent the element value of a whole brick, the differences between the surface element content and the internal element content must be verified.

The contents of 3 sections and the mean content of them are shown in Table S7 (Table S7). It is clear that the differences in the values between the sections and surface points were not much large for most cases. Max{Cp,Cs}/Min{Cp,Cs} for Fe, Al, and Si were lower than 1.3 for all bricks (Table S8). However, for K and Ca, there were a few cases whose Max{Cp,Cs}/Min{Cp,Cs} were higher than 1.3 (Table S8). The main reasons for this was that Ca and K were highly affected by crystalline bloom, while the elements Fe, Al, and Si were affected less by this phenomenon. However, it is impossible for in-situ measurement to cut up the bricks to evaluate the differences between the surface and interior. In regard to this phenomenon, it would be better to select a brick located on a higher position in the wall. In comparison to the bricks close to the ground, capillary suction of the wall at a higher position is much smaller [35]. Therefore, crystalline bloom at a higher position would be lighter, leading to a lesser impact on K and Ca. This can minimize the possibility of measuring bad data.

3.4 Correlation and linear regression analysis

In a previous study, several laboratory techniques, excluding ICP-OES [32, 36, 37], were used to perform cross-validation to assess the reliability of HH-XRF. Examples of such techniques are atomic absorption spectroscopy (AAS) [34], inductively coupled plasma mass spectrometry (ICP-MS) [18], and inductively coupled plasma atomic emission spectroscopy (ICP-AES) [38, 39].

For instance, certain researchers employed ICP-OES to perform cross-validation. In 2009, Radu assessed the reliability of HH-XRF using AAS, while certain other scholars employed ICP-MS and ICP-AES to conduct the comparison using HH-XRF.

In the present study, ICP-OES was employed to conduct the cross-validation of Fe, Ca, K, Al, and Si. XRF analysis targets all the atoms present within the limits of critical penetration depth, irrespective of the mineral structure. Aqua-regia hot-plate dissolution prior to conducting the ICP-OES analyses has been demonstrated to result in reduced recovery of elements, in certain cases, compared to the microwave extraction protocols incorporating hydrofluoric acid to break down the silicate phases. In this context, total microwave acid digestion, which is suitable for organic-rich and silicate-containing media with proven recoveries approaching 100%, was used to ensure maximum comparability between the HH-XRF and ICP data.

In order to verify the reliability of the HH-XRF results in the present study, Deming regression was used in the comparison between HH-XRF and ICP-OES values with HH-XRF placed on the x-axis and ICP-OES on the y-axis. As it incorporates errors on both x and y axes assuming the RSD is similar across the measurement range (Fig. 3) [40]. In case of Fe, Al, and Si elements, all the 20 bricks were used, while for K and Ca, 15 and 13 bricks were used, respectively, after removing certain cases in which either the surface was not uniform or the difference between the surface and the interior was huge. The contents of HH-XRF for each brick are the mean value of 10 points after treated by MPS.

In the case of Fe, Al, and Si, the coefficient of determination was greater than 0.85 (Fig. 3a and 3d-3e). In the case of K, the coefficient of determination was greater than 0.7 (Fig. 3c). The RSD for all these four elements model were lower than 10%. Combined with the inferential statistics (slope and intercept), all these four models fulfilled the requirements for a Q2 quality level, i.e., the relationship y = mx or y = mx + c was accepted.

In the case of Ca, even after removing certain values as stated in 3.3.1 and 3.3.2, the R^2 and RSD for this element reached only 0.63 and 17.0% (Fig. 3e).

To corrected the data of HH-XRF, Rotational (slope, m) and translational (intercept, b) bias were corrected for HH-XRF data by solving for ‘y’ in ‘y = mx+b’ for each regression model.

Relative proximity (RP=absolute (100-(HH-XRF value/ICP-OES value)×100)) is a useful indicator of inaccuracy as it demonstrates the proportional difference away from the reference value [41].

After the correction, the mean RP improved from 6.08% to 4.49% for Fe, 8.22% -7.33% for K, 6.05%-4.25% for Al and from 3.97% to 2.00% for Si measurements (Fig. 4 a1-d2). Although the regression model for Ca is at Q1 quality level, the RP still improved from 23.84%-11.20% after correction (Fig.4 f1 and f2).

When HH-XRF is used to perform the in-situ measurements of elements Fe, K, Al, and Si, a few bricks that have the same matrix as the target bricks should be selected to perform a preliminary experiment in order to conduct a Deming regression between HH-XRF and ICP-OES (or any other reliable laboratory method), which would provide a cross-validation correction for the values that were measured in situ.

4. Conclusions

It was concluded that HH-XRF is a reliable instrument for the in-situ determination of the main elements, with the exception of Ca. Owing to the complex conditions of bricks in situ and the characteristics of HH-XRF, a scientific method is necessary. The scientific suggestions for the application of HH-XRF in in-situ measurements provided in the present study are as follows.

Part 1 Recommendations related to the selection of the HH-XRF Analyzer

(1) Measurement time: The suggestions for measurement times for this application using Niton XL2–960 GOLDD XRF Analyzer are presented in Table 2. However, the instrument also has some influence on the

data. Therefore, if the instrument is not Niton XL2–960 GOLDD XRF Analyzer, it is essential to conduct preliminary tests on the object to determine the appropriate measurement time.

(2) Cross validation: In case of elements Fe, K, Al, and Si, a few bricks should be used in a preliminary experiment that would allow a Deming regression analysis between HH-XRF and ICP-OES (or any other reliable laboratory method), as it would provide cross-validation corrections for the values measured in situ.

Part 2 Recommendations for general conditions

(1) Criteria to select points, treat surface, and get final data: at least 10 points must be selected on each brick for measurement. Each point must be polished with a sickle prior to performing the measurement. After the measurement, if the uniformity meets the requirement (RSD≤10%, ≤1.3), using the mean content of the 10 points to represent the elemental content of the brick. If there are specific values, whose uniformity does not meet the requirements, they should be deleted.

(2) How to avoid the effect of rain: Selecting a sunny day, when it has not rained for the previous three days, is important. If it begins raining during the measurements, it is essential to halt the measurements and take the preliminary tests per hour after the rain to compare the contents measured after the rain and before rain until previous values are restored.

List Of Abbreviations

HH-XRF: Hand-Held X-ray fluorescence spectrometry;

ICP-OES: Inductively coupled plasma optical emission spectrometry;

RSD: Relative standard deviation;

R^2: Coefficient of determination

DM: Direct measurement;

MPS: Measurement after polishing by sickle;

PCA: Principal components analysis;

: The ratio of the maximum value to the minimum value of 10 points;

Max{Cp,Cs}/Min{Cp,Cs}:The ratio of the larger content of the point (mean of the 10 points) and section (mean of the 3 sections) to the smaller value of them;

AAS: Atomic absorption spectroscopy;

ICP-MS: Inductively coupled plasma mass spectrometry;

ICP-AES: Inductively coupled plasma atomic emission spectroscopy;

RP: Relative proximity

Declarations

Availability of data and materials

All data generated during this study are included in the article.

Competing interests

The author declares that they have no competing interests.

Funding

This work was supported by the National Natural Science Foundation of China [grant number 51778402].

Authors' contributions

All the authors contributed to the current work. ZXC and LZ planed and conducted the experiments and collected the data. ZXC and LZ performed the analyses and wrote the article. JLX assisted in experiment 3–1. FH supervised the entire process and provided constructive advice. All authors read and approved the final manuscript.

Corresponding authors:

Correspondence to Zexuan Chen or Long Zhang or Feng Hou.

Co-first authors:

Zexuan Chen and Long Zhang

Acknowledgements

None

Author details

[1] Tianjin International Engineering Institute, Tianjin University, Tianjin 300072, People's Republic of China.

[2] School of Architecture, Tianjin University, Tianjin 300072, People's Republic of China.

[3] Key Laboratory of Advanced Ceramics and Machining Technology of the Ministry of Education, School of Materials Science and Engineering, Tianjin University, Tianjin 300072, People's Republic of China.

References

1. Wang MB. The Linqing tribute brick. Root Exploration. 2007;14:92–7 **(in Chinese)**.
2. Li YJ. The Linqing tribute brick: The cornerstone of a capital. Inheritance. 2010;20:56–8 **(in Chinese)**.
3. Yan J. Study of the Historical and Material Pedigree of Linqing Brick. Master's Degree Thesis of Tianjin University; 2019 **(in Chinese with English abstract)**.
4. Zhai HY. A peliminary study of Linxi Chen kiln with Ming and Qing tribute brick. Journal of Xingtai University. 2015;30:22–4 **(in Chinese)**.
5. Wang YL. A Study of Kiln-Firing Production for Construction of Beijing in The Ming Dynasty: Focus on The Changes of Kiln Sites, Product Structure and Manufacture System of Supplies. Palace Museum Journal. 2012;55:21–71+161 **(in Chinese with English abstract)**.
6. Li X. The Mark of cinnabar ink on the Bricks of Beijing City. Oriental Collection. 2015;7:117–9 **(in Chinese)**.
7. Cai Q. The Analysis Of Precious Moulage Of Brick Beijing City Wall In Ming Qing Dynasty. Architecture & Culture. 2016;13:192–3 **(in Chinese with English abstract)**.
8. Song L. A Textual Research on the Ming Dynasty Tombs. Beijing: Forbidden City Press; Shanghai: Shanghai Culture Press; 1996. p. 296–301 **(in Chinese)**.
9. Phillips SC, Speakman RJ. Initial source evaluation of archaeological obsidian from the Kuril Islands of the Russian Far East using portable XRF. J Archaeol Sci. 2009;36 (6):1256–63.
10. Craig N, Speakman RJ, Popelka-Filcoff RS et al. Comparison of XRF and PXRF for analysis of archaeological obsidian from Southern Peru. J Archaeol Sci. 2007;34(12):2012–24.
11. Ruka R, Galaty ML, Riebe DJ et al. pXRF analysis of obsidian artifacts from Albania: Crossroads or cul-de-sac? .J Archaeol Sci: Rep. 2019;24:39–49.
12. Romano FP, Pappalardo G, Pappalardo L et al. Quantitative non-destructive determination of trace elements in archaeological pottery using a portable beam stability-controlled XRF spectrometer. X-Ray Spectrom. 2006;35(1):1–7.
13. Hunt AMW, Speakman RJ. Portable XRF analysis of archaeological sediments and ceramics. J Archaeol Sci. 2015;53:626–38.
14. Charalambous A, Webb JM. Metal procurement, artefact manufacture and the use of imported tin bronze in Middle Bronze Age Cyprus. J Archaeol Sci. 2020; 113(105047).
15. Vianello A, Tykot RH. Investigating Technological Changes in Copper-Based Metals Using Portable XRF Analysis. A Case Study in Sicily. Open Archaeol. 2017;3(1):392–408.
16. Simsek G, Unsalan O, Bayraktar K, Colomban P. On-site pXRF analysis of glaze composition and colouring agents of "Iznik" tiles at Edirne mosques (15th and 16th-centuries). Ceram Int. 2019;45(1):595–605.
17. Simsek G, Arli BD, Kaya S, Colomban P. On-site pXRF analysis of body, glaze and colouring agents of the tiles at the excavation site of Iznik kilns. J Eur Ceram Soc. 2019;39(6):2199–209.

18. Parsons C, Margui Grabulosa E, Pili E et al. Quantification of trace arsenic in soils by field-portable X-ray fluorescence spectrometry: Considerations for sample preparation and measurement conditions. J Hazard Mater. 2013;262:1213–22.
19. Nazaroff AJ, Prufer KM, Drake BL. Assessing the applicability of portable X-ray fluorescence spectrometry for obsidian provenance research in the Maya lowlands. J Archaeol Sci. 2010;37(4):885–95.
20. Goodale N, Bailey DG, Jones GT et al. pXRF: a study of inter-instrument performance. J Archaeol Sci. 2012;39(4):875–83.
21. Speakman RJ, Steven Shackley M. Silo science and portable XRF in archaeology: a response to Frahm. J Archaeol Sci. 2013;40(2):1435–43.
22. Frahm E. Characterizing obsidian sources with portable XRF: accuracy, reproducibility, and field relationships in a case study from Armenia. J Archaeol Sci. 2014;49:105–25.
23. Newlander K, Goodale N, Jones GT, Bailey DG. Empirical study of the effect of count time on the precision and accuracy of pXRF data. J Archaeol Sci: Rep. 2015;3:534–48.
24. Bonizzoni L, Galli A, Gondola M, Martini M. Comparison between XRF, TXRF, and PXRF analyses for provenance classification of archaeological bricks. X-Ray Spectrom. 2013;42:262–7.
25. Yang GM, Yang YZ, Yao ZQ et al. Study on Manufacturing Technique for Glazed Tiles Bodies from Mingzhongdu Site, Fengyang. Spectrosc Spect Anal. 2019;39(4):1280–7 **(in Chinese with English abstract)**.
26. Kang BQ, Li H, Miao JM. A Study on the Composition and Related Issues of Glaze of the Forbidden City in the Qing Dynasty. Cult Relics South China. 2013;52:67–71 **(in Chinese with English abstract)**.
27. Duan HY, Ding YZ, Liang GL. The chemical composition characteristic and firing technology research on ancient building glazed tile bodies in China. China Ceramics. 2011;47(4):68–72 **(in Chinese with English abstract)**.
28. US-EPA, Field Portable X-ray Fluorescence Analyzer: Metorex X-MET 920-P and 940, U.S. Environmental Protection Agency Office of Research and Development, Washington, DC, U.S., 1998.
29. Lemiere B. A review of pXRF (field portable X-ray fluorescence) applications for applied geochemistry. J Geochem Explor. 2018;188:350–63.
30. He WQ, Xiong YF. Quantitative analysis of ancient ceramic by X-ray spectroscopy techniques. Sciences of Conservation and Archaeology. 2003;15(3):13–20**(in Chinese with English abstract)**.
31. Zhang B. A Study of Application of PIXE to Provenance Determination of Ancient Ceramics and Glasses. Master's Degree Thesis of Fudan University; 2004 **(in Chinese with English abstract)**.
32. Kilbride C, Poole J, Hutchings TR. A comparison of Cu, Pb, As, Cd, Zn, Fe, Ni and Mn determined by acid extraction/ICP–OES and ex situ field portable X-ray fluorescence analyses. Environ Pollut. 2006;143(1):16–23.
33. Weindorf DC, Bakr N, Zhu Y et al. Influence of Ice on Soil Elemental Characterization via Portable X-Ray Fluorescence Spectrometry. Pedosphere. 2014;24(1):1–12.

34. Radu T, Diamond D. Comparison of soil pollution concentrations determined using AAS and portable XRF techniques. J Hazard Mater. 2009;171 (1–3):1168–71.
35. Zhang ZJ. Weathering mechanism and prevention methods of ancient brick in PingYao City, Shanxi Province, China. Journal of Engineering Geology. 2017;25(3):619–629 **(in Chinese with English abstract).**
36. Ridings M, Shorter AJ, Smith JB. Strategies for the investigation of contaminated sites using field portable X-ray fluorescence (FPXRF) techniques. Commun Soil Sci Plan. 2000;31(11–14):1785–90.
37. Shuttleworth EL, Evans MG, Hutchinson SM, Rothwell JJ. Assessment of Lead Contamination in Peatlands Using Field Portable XRF. Water Air Soil Poll. 2014;225(1844).
38. Wu C, Tsai H, Yang K, Wen J. How Reliable is X-Ray Fluorescence (XRF) Measurement for Different Metals in Soil Contamination? Environ Forensics. 2012;13(2):110–21.
39. Arenas L, Ortega M, Garcia-Martinez MJ, Querol E, Llamas JF. Geochemical characterization of the mining district of Linares (Jaen, Spain) by means of XRF and ICP-AES. J Geochem Explor. 2011;108(1):21–6.
40. Rouillon M, Taylor MP. Can field portable X-ray fluorescence (pXRF) produce high quality data for application in environmental contamination research? Environ Pollut. 2016;214:255-64.
41. Rouillon M, Taylor MP, Dong C. Reducing risk and increasing confidence of decision making at a lower cost: In-situ pXRF assessment of metal-contaminated sites. Environ Pollut. 2017;229:780-9.

Figures

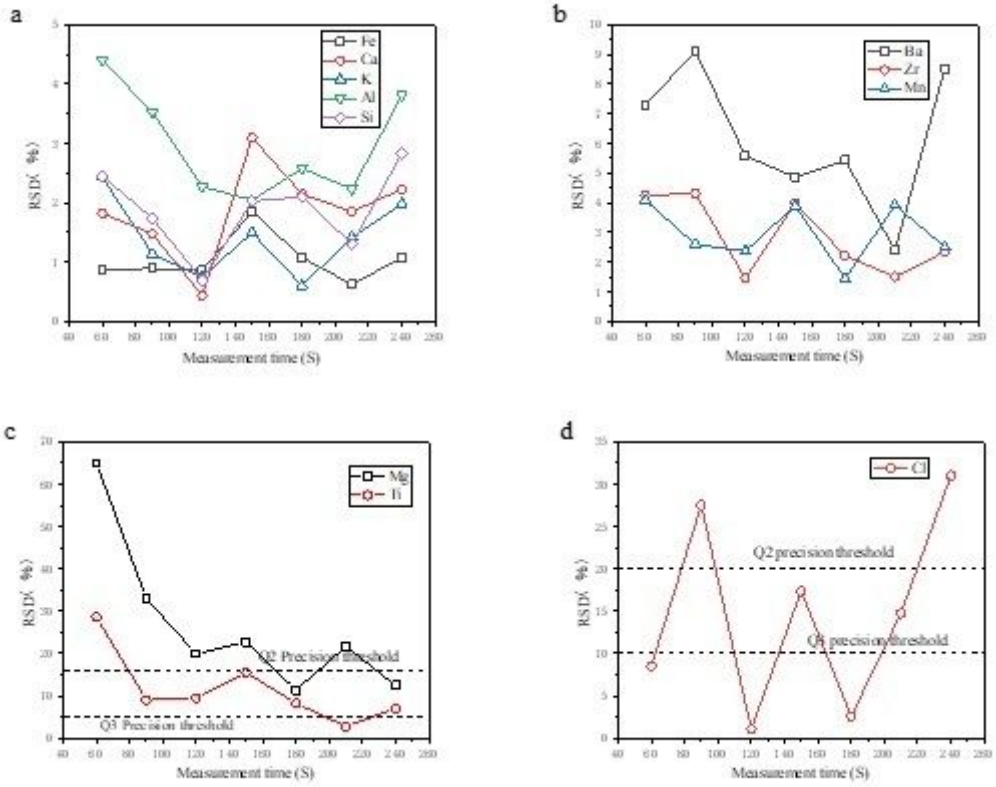

Figure 1

Relationships between measurement time and RSD on precision for Fe, Ca, K, Al, Si, Ba, Zr, Mn, Mg, Ti, and Cl. The brick used was measured 5 times at 1 point for each measurement time. The RSD shown are calculated from these 5 replicates. Raw data shown in Table S9

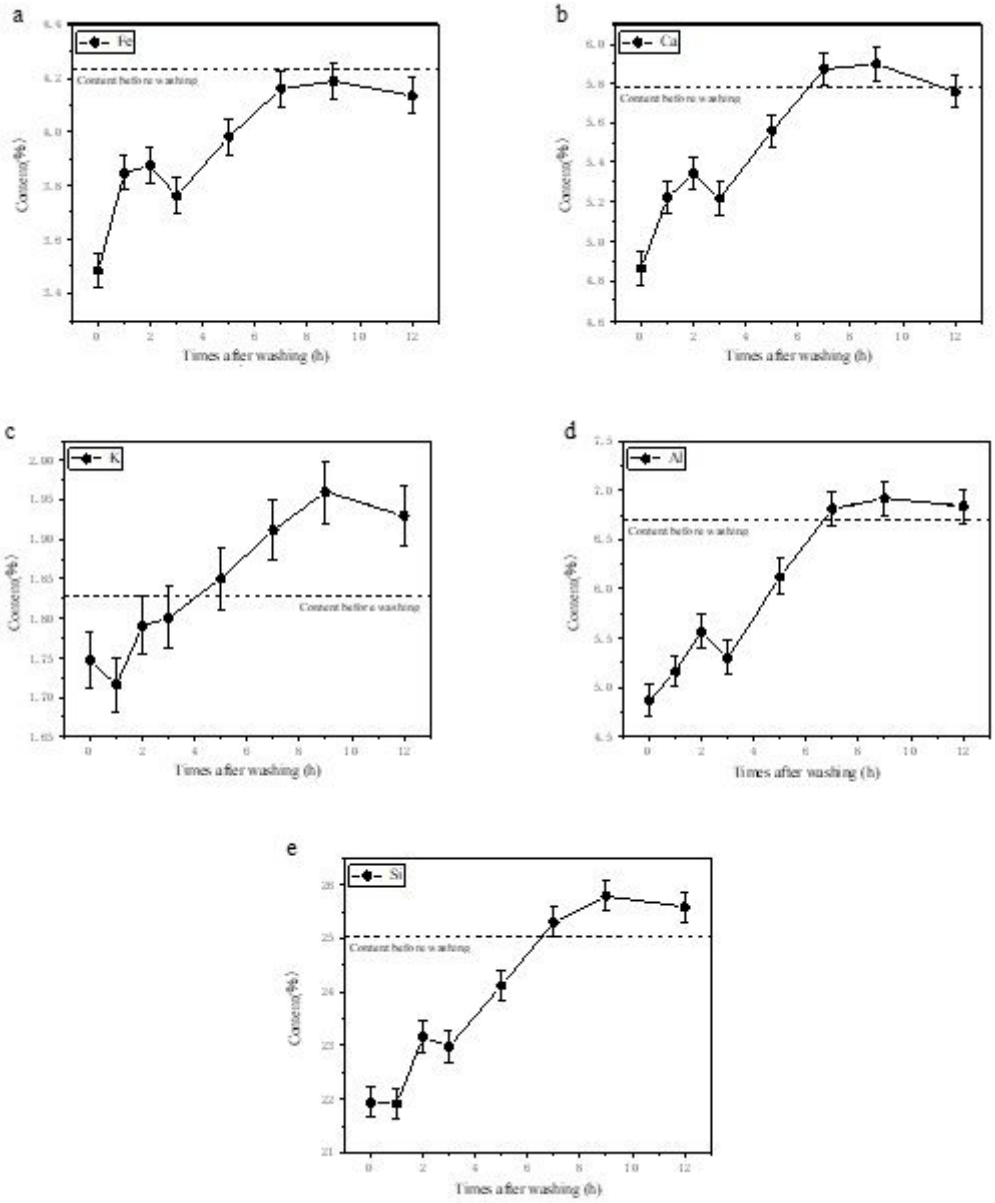

Figure 2

Variety of contents of each element and their comparison with the contents before being washed. Error bars = 5%

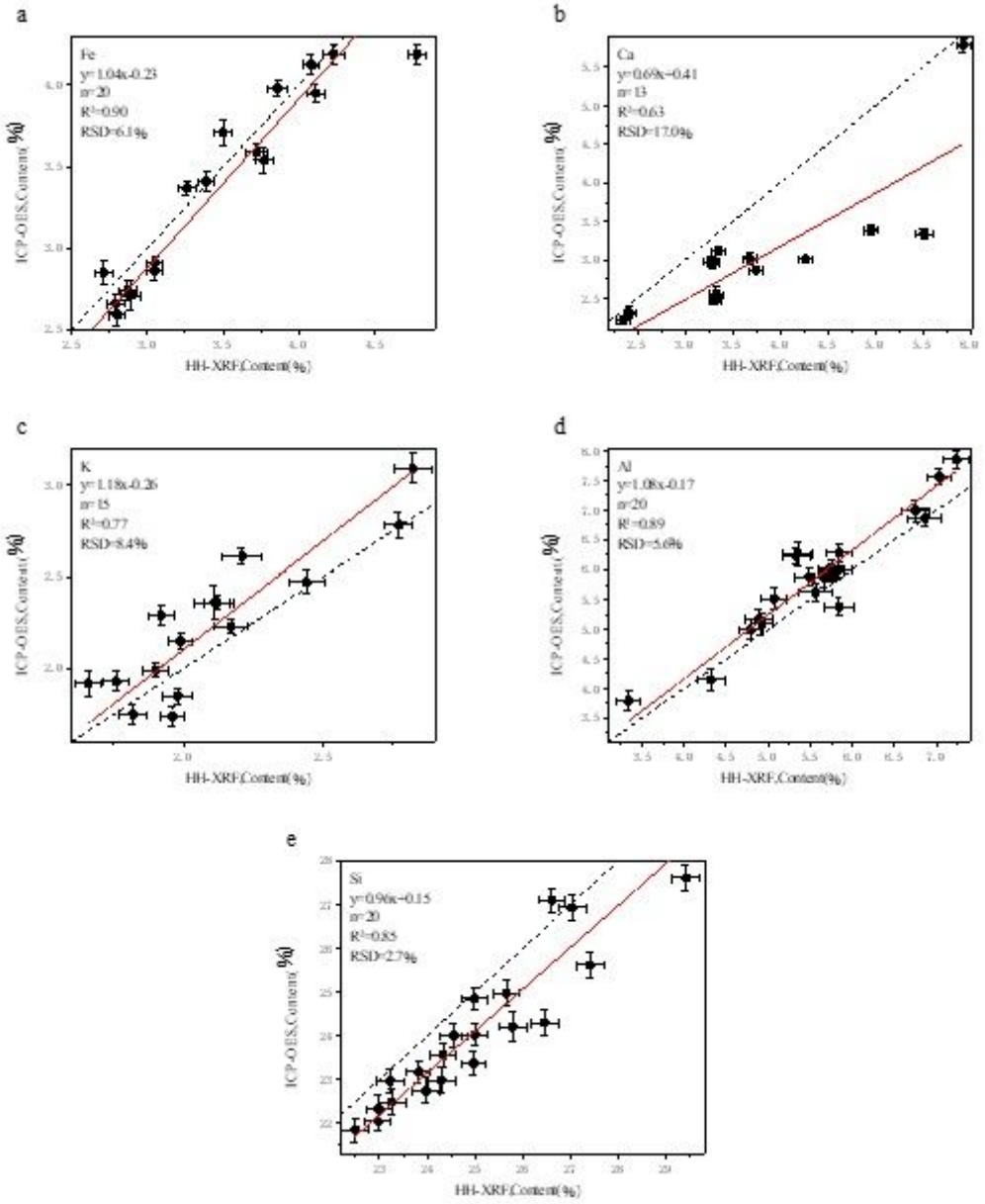

Figure 3

Regression of HH-XRF measurements against ICP-OES analysis. Deming relationship (solid red line) and 1:1 (dashed black line) are shown in each plot. X error bars = 5%, Y error bars = 5%.

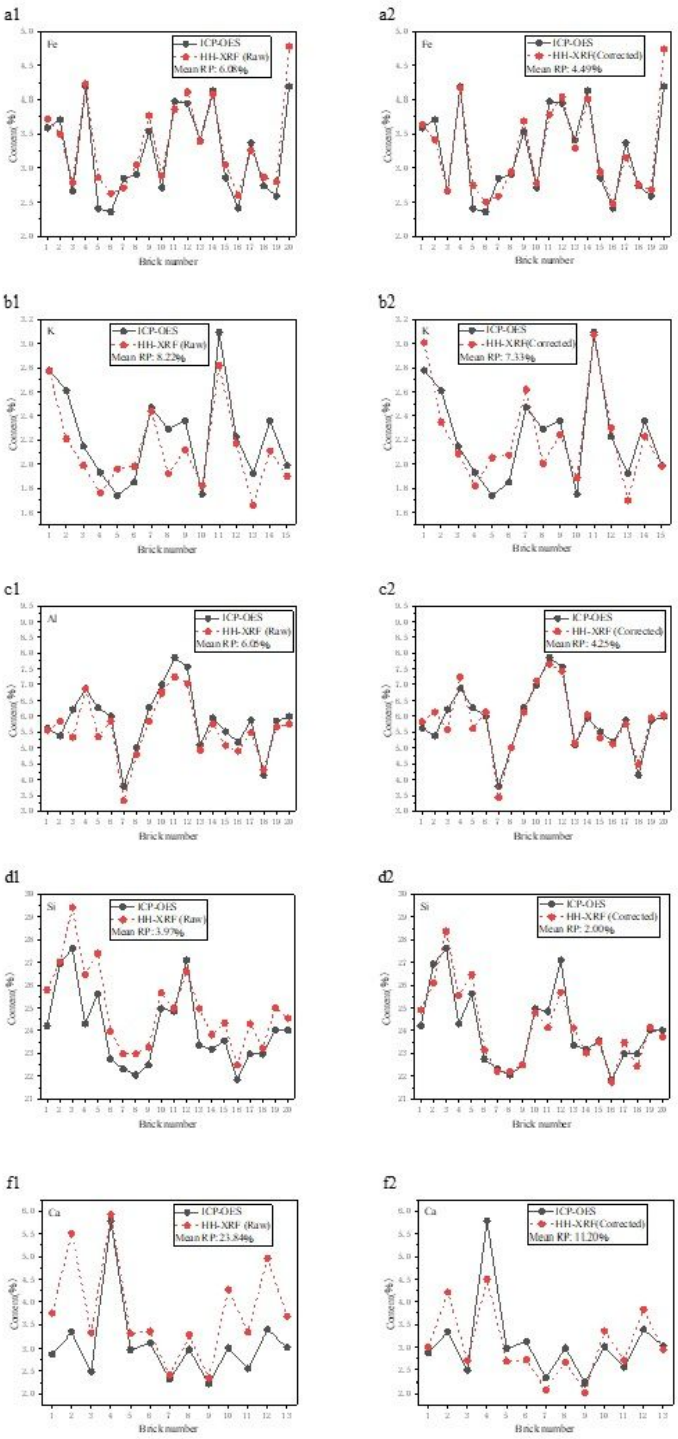

Figure 4

Point by point graphs of HH-XRF measurements against ICP-OES data. Impact of in-situ HH-XRF data adjustment using ICP-OES data is demonstrated between pre- and post-correction rows. Relative proximity (RP) gives an indication of HH-XRF inaccuracy when compared to a reference value (ICP-OES data) and is calculated by RP = absolute (100-recovery value×100)